Integrative Biology

Quantitative biosciences from nano to macro
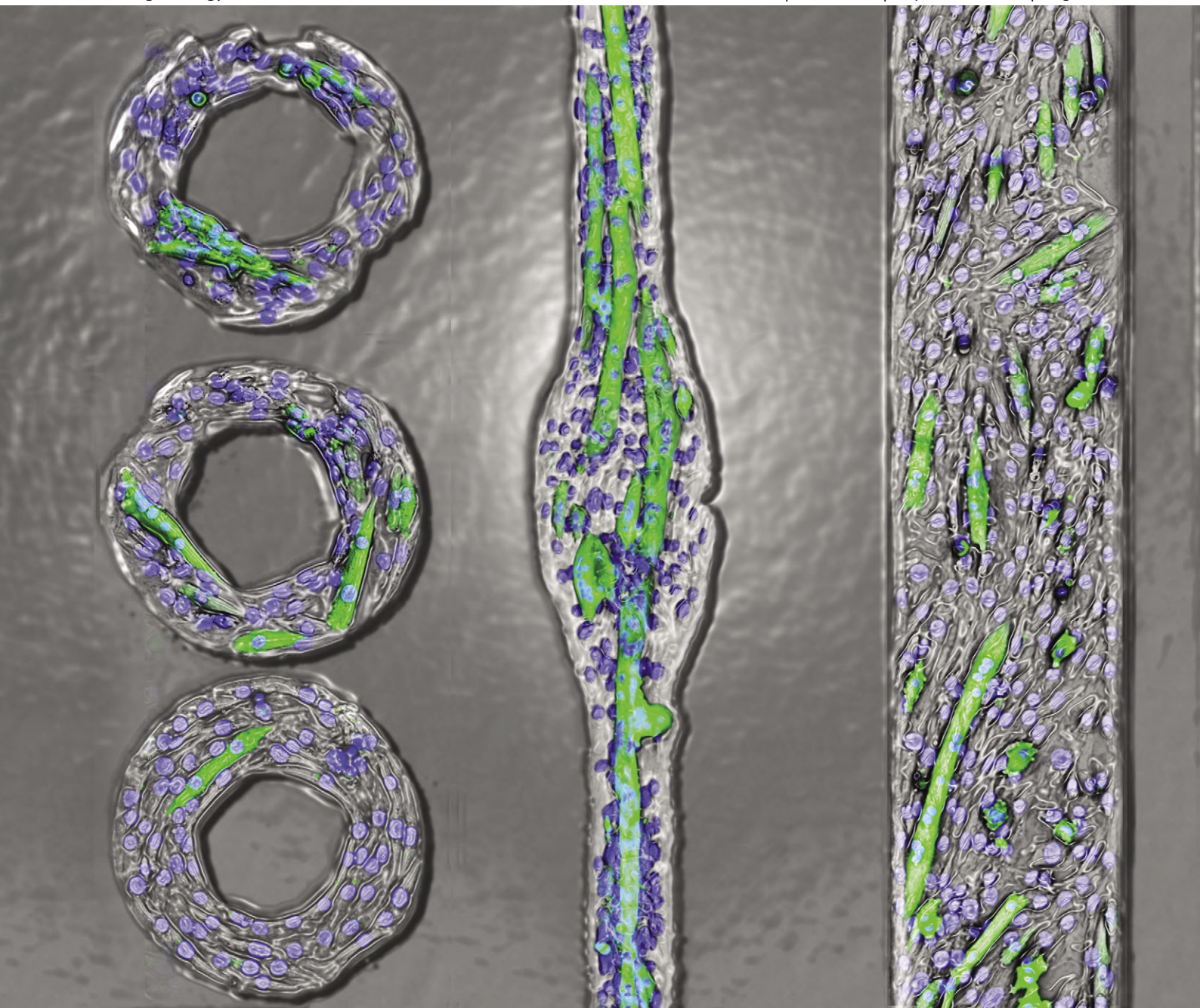
RSC Publishing

PAPER
Bajaj and Bashir
Patterning the differentiation of C2C12 skeletal myoblasts

Patterning the differentiation of C2C12 skeletal myoblasts†

Piyush Bajaj,[ab] **Bobby Reddy Jr.,**[bc] **Larry Millet,**[bc] **Chunan Wei,**[c]
Pinar Zorlutuna,[abd] **Gang Bao**[e] **and Rashid Bashir***[abc]

Mammalian cells are sensitive to the physical properties of their micro-environment such as the stiffness and geometry of the substrate. It is known that the stiffness of the substrate plays a key role in the process of mammalian myogenesis. However, the effect of geometrical constraints on the process of myogenic differentiation needs to be explored further. Here, we show that the geometrical cues of substrates can significantly influence the differentiation process of C2C12 skeletal myoblasts. Three different geometries including lines of different widths, tori of different inner diameters, and hybrid structures (linear and circular features with different arc degrees) were created by micro-contact printing of fibronectin on the surface of Petri dishes. The differentiation of C2C12 cells was studied over a period of seven days and was quantified; we report the differentiation parameters of (1) fusion index, (2) degree of maturation, (3) alignment, and (4) response to electrical pulse stimulation (EPS). Hybrid structures with the smallest arc degree (hybrid 30°) showed the best results for all four differentiation parameters. The hybrid 30° pattern exhibits an ∼2-fold increase in the fusion index when compared to the line patterns and an ∼3-fold increase when compared to the toroid patterns. The hybrid 30° also showed a higher maturation index compared to the line or the toroid patterns. In response to electrical stimulation (20 V, 50 ms pulse, 1 Hz), mature myotubes on hybrid 30° patterns showed an ∼2-fold increase in cellular displacement when compared to myotubes on the line and torus patterns. We tested the influence of C2C12 cell density on fusion and maturation indices, and the results suggest that density does not exert significant influence on cellular differentiation under these conditions. Our results can have important implications in engineering skeletal muscle tissues and designing muscle cell bio-actuators.

[a] *Department of Bioengineering, University of Illinois at Urbana-Champaign, Urbana, IL 61801, USA.*
E-mail: rbashir@illinois.edu; Fax: +1 217 244-6375;
Tel: +1 217 333-3097
[b] *2000 Micro and Nanotechnology Laboratory, University of Illinois at Urbana-Champaign, 208 North Wright Street, Urbana, IL 61801, USA*
[c] *Department of Electrical and Computer Engineering, University of Illinois at Urbana-Champaign, Urbana, IL 61801, USA*
[d] *Now at Harvard-MIT's Division of Health Sciences and Technology, Massachusetts Institute of Technology, Cambridge, MA 02139, USA*
[e] *Department of Biomedical Engineering, Georgia Institute of Technology and Emory University, Atlanta, GA 30332, USA*
† Electronic supplementary information (ESI) available. See DOI: 10.1039/c1ib00058f

Introduction

Cells and tissues are exposed to a variety of mechanical forces during different physiological processes.[1] For example, skeletal muscles are in a constant state of tension during exercise and walking, endothelial cells experience shear stress because of the blood flow through the vessels and cardiac muscles respond to both shear stress and tension. Techniques such as micro-contact printing (μCP) have enabled researchers to print organic molecules on surfaces and study cell–cell and cell–surface interactions, and thereby develop models to understand force sensing by cells.[2–5] Landmark studies have shown that it is

Insight, innovation, integration

Micropatterning techniques have enabled researchers to print organic molecules on substrates thereby regulating the location and shape of cells on them. These techniques have been widely used to mimic the complex three-dimensional *in vivo* tissue architecture and enabled us to gain deeper understanding about the physiological micro-environment experienced by the cells. In this study, using micro-contact printing, we show that the differentiation of the murine-derived skeletal muscle cell line, C2C12 myoblasts, is closely dependent on the shape of the protein islands. The use of micropatterning techniques helped us to decouple the geometrical (mechanical) cues experienced by the cells *in vitro* which otherwise are uncontrolled under classic cell culture conditions.

possible to control the fate of the cell solely by controlling the geometry of the underlying substrate.[6] Similarly, it has also been shown that the cell shape (because of the underlying geometry) regulates the commitment of the human mesenchymal stem cells (hMSCs); cells when allowed to spread and flatten undergo osteogenesis while round, balled-up cells become adipocytes.[7] Using μCP, it has also been shown that even in the same geometrical structure, hMSCs at the edges or corners of the micropatterned protein islands differentiate into osteogenic lineages while those at the center of the structure become adipocytes.[8] In addition, endothelial and epithelial cells cultured on micropatterned protein islands show increased proliferative/growth rates at the corners than at the center of these structures because of the greater stresses at the corners than at the center.[9] Thus these and several other studies accurately concluded that mechanical forces play a key role in modulating cellular behavior like migration, proliferation, division, gene expression and apoptosis.[10–21] Building on these prior studies, we became interested in examining how geometrical cues can be orchestrated to maximize the differentiation of C2C12 mouse myoblast cells into myotubes.

When deprived of serum, C2C12 cells undergo cell cycle arrest and fuse together to form multi-nucleated myotubes.[22–24] C2C12 cells are used as a model system to study different types of muscular dystrophies like Duchenne muscular dystrophy (DMD), Emery–Dreifuss muscular dystrophy (EDMD) and limb–girdle muscular dystrophy (LGMD) in vitro.[25–27] Studies have described the micro-patterning of C2C12 cells; for instance, micro-patterning has been used for creation of single myotubes on thermally responsive surfaces.[28] The C2C12 myotube/fibrin gel system has been developed to show that the cells in fibrin gels elicit greater contractile activity than C2C12 cultures on conventional two-dimensional surfaces.[29] Two-dimensional muscle syncytia have been developed on glass to show actin fiber alignment after myotube formation.[30] The optimal width of patterns for the formation of single myotubes has been found to be around 30 μm[31] and various studies have shown the alignment of myotubes on nanofibrous and micropatterned polymers.[18,32,33] However, none of these studies aimed at finding an optimum geometry to simultaneously enhance the differentiation, alignment and functionality of myotubes.

Maximizing the differentiation and alignment of cells in the tissue/biomaterial is fundamental for engineering functional tissues with anisotropic properties.[34] It has been previously shown that regulation of the RhoA and ROCK pathway is required for skeletal muscle differentiation.[35,36] Also, it is known that the Rho/ROCK pathway is involved in stress sensing and cytoskeletal organization in cells.[37] Therefore, we hypothesized that different morphologies of protein micro-patterns could confer changes in tractional stresses and cytoskeletal organization of C2C12 myoblasts thereby modulating cellular differentiation.

The overall architecture of tissues in the body does not follow only linear or circular geometries; rather it is an amalgamation of linear and circular patterns. Therefore, in this study, three different geometries including lines of different widths, tori of different inner diameters, and hybrid structures (combining linear and circular features with different arc degrees)

were created by μCP of fibronectin. The hybrid 30° pattern of all the different geometries showed the best results for fusion, maturation, alignment, and cellular displacement of myotubes. It was verified that these results cannot be attributed to the different densities of cells on the various micropatterns, suggesting that the different geometries induce changes in the cytoskeletal organization or gene/protein expression. This study has implications not only for skeletal tissue engineering but for design of actuators in biological micro electromechanical systems (BioMEMS) where the anisotropy of tissues is required for a functional outcome.

Experimental

Fabrication of micropatterned substrates

Fig. 1A shows a schematic overview of the entire μCP process. SU-8 (Micro Chem, Newton, MA) masters were created on a silicon wafer by using standard photolithography. The master was first silanized by dimethyl (3,3,3-trifluoropropyl) silane (Sigma, St. Louis, MO) and polydimethylsiloxane (PDMS) stamps were replicated from the master by casting Sylgard 184 (Dow Corning, Midland, MI) on the silicon wafer. Micro-patterned substrates were prepared by stamping the PDMS on 35 mm Falcon polystyrene Petri dishes (BD Biosciences, Bedford, MA). The PDMS stamp was coated with 50 μg ml^{-1} of fibronectin (Sigma, St. Louis, MO) and incubated for 30 min prior to stamping them on the Petri dishes. The stamps were then dried with nitrogen and kept in conformal contact with the substrate for 20 min in an incubator. After stamping the protein, the substrate was blocked with 2% Pluronic F-127 (Sigma, St. Louis, MO) to render all unpatterned regions non-adhesive to the cells. The substrate was rinsed three times with phosphate buffered saline (PBS, Lonza Inc., Williamsport, PA) prior to cell seeding. Approximately, 75 000 cells were seeded on each substrate and observed for nine days resulting in an initial cell seeding of 7800 cells per cm^2 for the 35 mm Petri dish. We patterned three different geometries, with multiple sized structures for each geometry. For linear patterns, we used 2000 μm long lines of various widths (300 μm, 150 μm, 80 μm, 40 μm, 20 μm, and 10 μm). Torus patterns consisted of the various inner diameters (ID) (40 μm, 100 μm, and 200 μm) and outer diameters (OD) (200 μm, 260 μm and 360 μm). Hybrid patterns were fabricated to produce a linear element with a central circular belly; the linear element was 100 μm wide, whereas the arc of the circular belly was either 30°, 60° or 90°. The fourth, unpatterned substrate (control) was the unpatterned Petri dish.

Cell culture

The murine-derived muscle cell line (C2C12) was purchased from American Type Culture Collection (ATCC, Manassas, VA). The cells were cultured in Dulbecco's modified Eagle's medium (DMEM, Mediatech, Manassas, VA) supplemented with 10% fetal bovine serum (FBS, Sigma, St. Louis, MO) (growth medium, GM) and antibiotics. To induce the differentiation of myoblasts into myotubes, C2C12 cells at 80–90% confluency were shifted to DMEM supplemented with 2% horse serum (Lonza Inc., Williamsport, PA) (differentiation medium, DM) and the
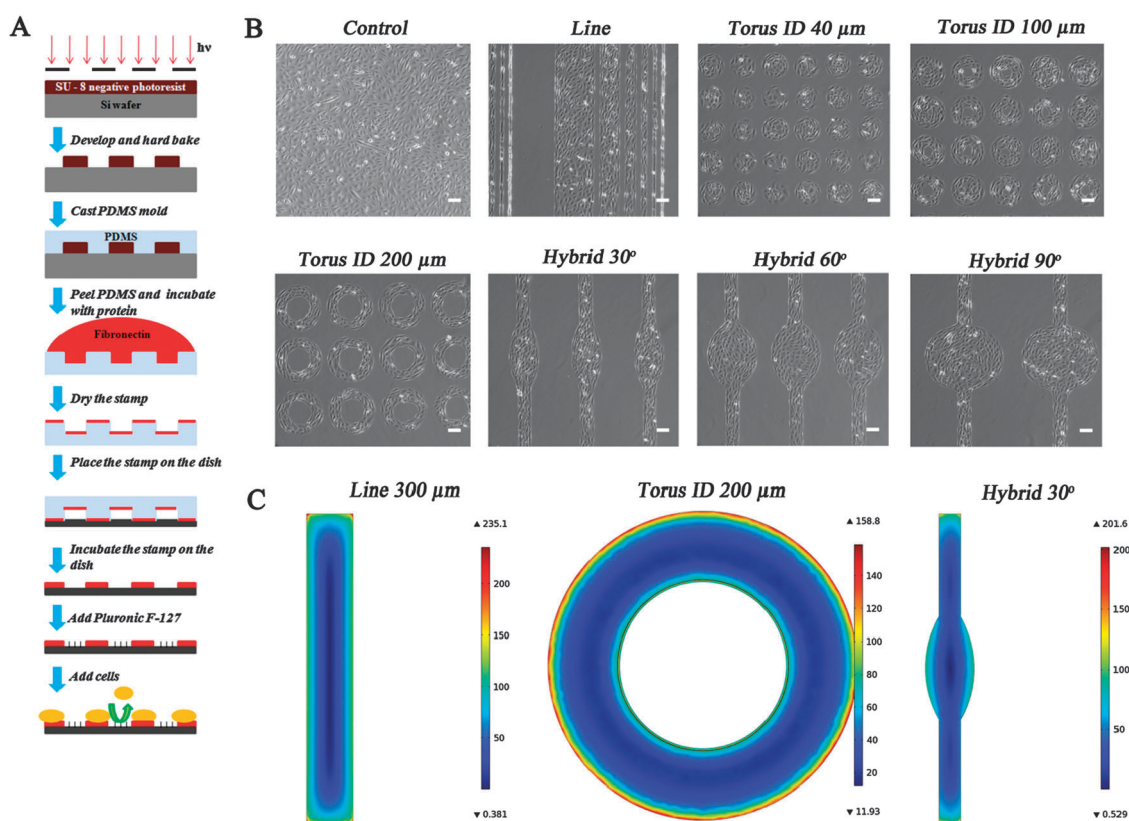
Fig. 1 Generation and characterization of the micropatterned substrates. (A) Schematic showing the preparation of the micropatterned substrates. (B) Phase contrast images of the different micropatterned cell islands used in the study—lines of different widths (300 μm, 150 μm, 80 μm, 40 μm, 20 μm, and 10 μm), tori of different inner diameters (40 μm, 100 μm, and 200 μm), and hybrid patterns of different arc degrees (30°, 60° and 90°). (C) von Mises stress patterns of the three different types of cell islands determined using finite element analysis (FEA). The von Mises stresses shown here are color-coded: red represents regions of maximum stress and blue represents those of minimum stress. The maximum stresses are concentrated at the corners or the periphery of the structures independent of their shape. (Scale bar = 100 μm.)

medium was replaced every other day. All the time points in the figures refer to cells present in the DM.

Generation of mechanical stress patterns of the micropatterned cell islands

Finite element analysis (FEA) was used to create the stress patterns of the micropatterned cell islands. A three-dimensional model for each type of cell island was created using COMSOL 4.1 (Palo Alto, CA). The two components used consist of a contractile layer and a passive layer as defined previously.[9,38] The bottom of the passive layer was fixed and contractility of the cells was simulated by induction of a thermal strain on the top layer. Both the bottom (passive) and the top (contractile) layers were assumed as isotropic materials with a Poisson's ratio of 0.499 and a Young's modulus of 100 and 500 Pa respectively. The co-efficient of thermal expansion for the top layer was 0.05 K^{-1} and its thermal conductivity was 10 $W\ m^{-1}\ K^{-1}$. In order to simulate contraction, a temperature drop of 5 K was prescribed on the top contractile layer. The ratio of the height of the contractile layer to the passive layer was 5 : 1 and other dimensions were prescribed by the geometry of the micropatterned islands. The von Mises stresses at the bottom of the passive layer are reported in this study. Thermal stress analysis was used as an analog to simulate the tractional stresses experienced by the cell.

Fig. S1 (ESI†) shows the deformation of the two-component cell model and the resultant von Mises stress on the different structures. Meshes of different sizes (minimum mesh size varied from 0.4–8 μm) were used to confirm the convergence of the results.

Immunofluorescence microscopy and quantitative analysis of myotubes

Differentiated C2C12 cells were fixed with 4% paraformaldehyde (PFA, Electron Microscopy Sciences Hatfield, PA) for 20 min and permeabilized with 0.2% Triton X-100 (Sigma, St. Louis, MO) for 10 min. The cells were blocked with 1% bovine serum albumin (BSA, Thomas Scientific, Swedesboro, NJ) solution for 30 min in PBS. All the previous steps were performed at room temperature. The cells were incubated with MF-20 (anti-myosin heavy chain (MHC), Developmental Studies Hybridoma Bank (DSHB), University of Iowa, IA) overnight at 4 °C followed by incubation with fluorescein isothiocyanate (FITC) conjugated anti-mouse IgG (Invitrogen, Carlsbad, CA) and DAPI (Invitrogen, Carlsbad, CA) in dark at 37 °C. The stained cells were imaged with a fluorescent microscope (IX81, Olympus, Center Valley, PA) and the images were quantified using ImageJ 1.42q.[39] The images obtained from the MHC and DAPI signals were pseudo-colored green and blue respectively.

Calculation of fusion index, maturation index and density for the myotubes

The fusion index was calculated as the ratio of the nuclei number in myocytes with two or more nuclei *versus* the total number of nuclei.[40] The maturation index was defined as myotubes having five or more nuclei.[40] Edges and regions which did not show good stamping or cell adhesion were not used for analysis. Cell density was calculated by dividing the number of cells in each pattern (counting the nuclei) by the area of the pattern (Table S1 in the ESI†). Two Petri dishes for each of the eight different patterns were used. At least five patterns on each dish were used for quantitative analysis. The sample size is also mentioned in the figure legends. The graphs were created in OriginPro 8.5, and Photoshop CS5 was used for assembly of figures for publication.

Electrical stimulation of myotubes

The contraction of myotubes was achieved by stimulating the cells with a pulse train using a custom-built electrical setup. Fig. S2 (ESI†) shows the setup used for the contraction studies. Platinum electrodes (diameter = 0.762 mm) spaced 1.2 cm apart were connected to the custom built setup and an Agilent waveform generator (Santa Clara, CA) was used for generating the pulses. To minimize electrolysis, a 220 μF capacitor (C) was connected in series to the circuit so that the resultant signal is produced with alternating polarity.[41] The Nyquist criterion, which states that the sampling frequency must be at least twice the highest frequency contained in the signal, was maintained during all video image acquisition. The resistance of the Petri dish with 1.5 ml of differentiation media (R_{media}) was calculated to be 475 Ω. The reactance at 1 Hz was calculated to be 725 Ω. Therefore, the net impedance of the equivalent circuit was calculated to be 865 Ω where the current leads the voltage by 56.71°. The impedance of the circuit at 1 Hz was calculated by assuming an RC circuit in series with the previously noted values for R_{media} and C. The time constant (τ) of the circuit was about 105 ms and the intensity of current in the circuit was calculated to be 15.5 mA. The resistance of the Petri dish with differentiation media was calculated using the relation $\tau = R_{media}*C$. The value of τ was obtained from the oscilloscope as one τ corresponds to the voltage dropping to 36.8% of the original (source) voltage. To actuate and measure myotube displacement, an electrical pulse (amplitude 20 V, duration 50 ms and frequency 1 Hz) was applied to the culture.

Analysis of alignment and cellular displacement

The alignment of myotubes in the micropatterned cell islands was quantified using a two-dimensional fast Fourier transform (FFT). The two-dimensional FFT function converts the information in an image from a "real" space into a mathematically defined "frequency" space which can then be used to look at the rate of change of pixel intensity across the entire image. The resulting FFT output image contains pixels that are arranged in a pattern that reflects the degree of alignment in the original image. The low frequency pixels which also represent the background and the overall shape of the image are placed at the center. The high frequency pixels which represent edges,

finer not repeated details and noise in the image are dispersed in a symmetrical pattern about the origin towards the periphery. These pixel intensities are summed along the radius for each angle of the circular projection and plotted against the corresponding angle of acquisition to produce a two-dimensional FFT alignment plot. The height and the overall shape of the peaks represent the degree of alignment of cells in the original image. A high and narrow peak indicates a more uniform degree of alignment while a broad peak indicates that more than one axis of alignment may be present. A completely random alignment is shown by no discernable peak in the alignment plot.

The process of extraction of the principal frequency from the movies captured by the camera is shown in Fig. S3, ESI.† First, a kymograph was generated from the image sequence. Second, the time-varying intensity of the kymograph was recorded. Third, an FFT function was applied to the resulting grayscale intensity values to generate a frequency spectrum. This spectrum represented the principal frequencies of myotube contraction. In order to detect the displacement of the myotubes, quantum dots (QDs) (Qtracker® 585 Cell labeling kit, Invitrogen, Carlsbad, CA) were loaded in the cell to create a good contrast so that a semi-automated approach could be used for quantification. Digital image correlation (DIC) was used to compute the displacement field of the cells and a routine was written in MATLAB R2009a (MathWorks, Natick, MA). Fig. S4 (ESI†) shows the C2C12 myoblasts/myotubes loaded with QDs and the approach used for detecting the displacement. A modified approach inspired by Kamgoué *et al.* was used.[42] A series of image files was generated from the individual frames of each movie, each separated by 0.21 s. The image files displayed good contrast between the QDs of interest and the background noise. In order to simplify the detection algorithm, noise thresholding was performed; all pixels below the noise thresholding value were set to a pixel value of 0. The first frame from each movie was used as Image 1, while all subsequent frames were used as Image N, where N is the frame number. A rectangular region of interest (ROI) was carefully chosen around each QD to be interrogated in Image 1, including approximately 10 μm of surrounding pixels to encompass displacement for the entirety of the movie. A window (Win 1) inside this ROI was selected tightly around each QD, chosen to minimize the amount of non-QD pixels. The coordinates and intensity of each pixel in Win 1 were recorded in the matrix $I_1(i, j)$. For each subsequent image, the same ROI was interrogated to locate the most similar subset to Win 1. This target subset was called *Win N* and was represented by the matrix $I_N(i + u_N, j + v_N)$, where u_N and v_N designate the desired displacement values to be extracted for Image N. *Win N* was located by sweeping the matrix $I_N*(i + u*, j + v*)$ through the ROI in Image N; each I_N* describes a temporary window *Win N** of the same size and shape as *Win 1*. Due to the very good contrast between QD pixels and non-QD pixels, we were able to consistently locate the target *Win N* by selecting the *Win N** of maximum mean intensity in the ROI:

$$I_N(i + u_N, j + v_N)$$
$$= \max\{\text{mean}(I_N*(i + u*, j + v*))\}|(u*, v*) \text{ in ROI} \quad (1)$$

The vectors u_N and v_N could then be correlated with the time value matching each frame N to construct the displacement *versus* time curves shown in Fig. 6.

The ROI in Image 1 must be chosen carefully to include the expected displacement for all frames in the movie sequence while minimizing selection of unwanted pixels (which can be either noise or adjacent QD not under interrogation). With proper selection of the ROI, we tested the automated displacement measurement method with several test sequences of images and determined the average error to be less than 1 pixel (around 0.285 μm).

Statistical analysis

Statistical analysis was performed using one-way ANOVA *post hoc* Tukey—means comparison in OriginPro 8.5. All data values reported in the study are mean ± standard error of the mean (S.E.M.).

Results

C2C12 myoblast micropatterning and stress map analysis of cell microislands

Skeletal myogenesis is a highly orchestrated terminal differentiation process in which the proliferating mono-nucleated myoblasts differentiate and fuse to form multi-nucleated myotubes. In this study, we investigated the influence of two-dimensional geometrical cues on the differentiation of C2C12 myotubes. C2C12 myoblasts were patterned on fibronectin islands using μCP. The cells on different types of geometries are shown in Fig. 1B after 24 hours of culture in GM. The cells conform uniformly to the protein microislands and form a confluent monolayer by the end of 24 hours. However, cells on the smallest torus pattern (torus ID 40 μm) blend over the central hole to form a circle rather than a torus. This effect was inversely related to the ID and was lessened for increasing ID's from 40 μm to 200 μm. Fig. 1C shows the von Mises stress at the fixed side of the bottom passive layer for the three different geometries—linear (300 μm), circular (ID 200 μm, OD 360 μm) and hybrid (arc degree 30°). The predicted von Mises stress patterns from the FEA model matched well with previous reports on the equivalent principal stress of similar structures.[9,38] The linear structure (line 300 μm) showed higher stresses at the edges than at the center and this stress value was maximized at the corners. Similarly, the torus (ID 200 μm, OD 360 μm) showed higher stress at the convex outer edge of the structure than at the concave inner edge. The stress distribution in the hybrid structure was at its maximum at the corners of the linear portion while the circular portions showed higher stresses than the center of the structure. In general, the perimeter of the structures showed higher stresses than the inner regions.

Fusion and maturation indices of C2C12 myoblasts on the different geometries

C2C12 myoblasts when deprived of serum undergo cell cycle arrest and start to fuse together to form multinucleated myotubes. Myotubes serve as the building blocks for skeletal muscle, thus understanding the differentiation process of C2C12 skeletal myoblasts *in vitro* has the potential to resolve

mechanisms of the myogenic differentiation process *in vivo* as well. Fig. 2 shows the fluorescent images of the cells present on the different patterns on days 1, 4 and 7 in DM; cells were cultured in GM for ∼24 hours and then switched to DM. As shown here, the myocyte differentiation increased as a function of time on all the substrates reaching a maximum by day 7 while nearly half of the toroid patterns showed very little to no differentiation even by day 7. Massive myotube detachment was seen on all substrates starting from ∼8–9 days in the differentiation media, a result that has been reported previously.[43,44]

To quantify the differentiation of myotubes, we calculated the fusion index from the immunofluorescent images by determining the number of nuclei in the MHC stained region (only regions with ≥ 2 nuclei were used) to the total number of nuclei in the field of view. At least two independent experiments were performed and the data shown here are from one of those two experiments which is representative of the two experiments. Fig. S5 (ESI†) shows the data combined for the two experiments for the fusion index. Fig. 3A shows the fusion index of the C2C12 cells on hybrid patterns. The results show a progressive decrease in myotube differentiation starting with the hybrid 30° followed by hybrid 60° and hybrid 90°. Hybrid 30° (45.38 ± 2.57%) showed greater than 1.5 fold differentiation compared to hybrid 60° (29.20 ± 1.20%) and hybrid 90° (25.71 ± 2.62%). In contrast, there was no significant difference in the differentiation of C2C12 myotubes on the linear patterns of different widths (Fig. 3B). However, myotubes on the linear patterns showed a significant decrease in differentiation when compared to the control at $p < 0.01$. The large width line pattern (300 μm) was used to mimic the unpatterned control. Presumably, even thicker patterns are required so that the cells on these patterns start mimicking the properties of the cells on the unpatterned control. Similar results were observed for the circular geometry. There was no significant difference of differentiation between the toroids of different IDs; when compared to controls, all of the toroids showed a decrease in differentiation (Fig. 3C, $p < 0.01$). Fig. 3D summarizes the fusion index for all the different geometries by incorporating the highest for each type.

The results suggest that adding a small degree of circularity to a linear structure (hybrid 30°) enhances the differentiation of C2C12 myoblasts into myotubes. This geometry showed the highest fusion index of all the different patterns used. The next highest fusion index was observed for the linear geometry while the circular geometry (torus) showed the lowest fusion index of all the patterns in this study.

The maturation index (% myotubes ≥ 5 nuclei) was also used as a parameter to evaluate the differentiation of C2C12 myotubes. The maturation index can also be used to quantify the size of the myotube, a higher maturation index represents a myotube which is larger in size.[40] The maturation index of the hybrid patterns is shown in Fig. 4A. It can be seen that the hybrid 30° pattern, which showed the highest fusion index, also shows the highest maturation index for the myotubes. The maturation index for the hybrid 30° (73.09 ± 4.41%) pattern was statistically higher ($p < 0.05$) than that for the control (60.24 ± 2.19%), hybrid 60° (55.11 ± 3.83%) and hybrid 90° (46.71 ± 3.91%) ($p < 0.01$). Fig. 4B shows the maturation
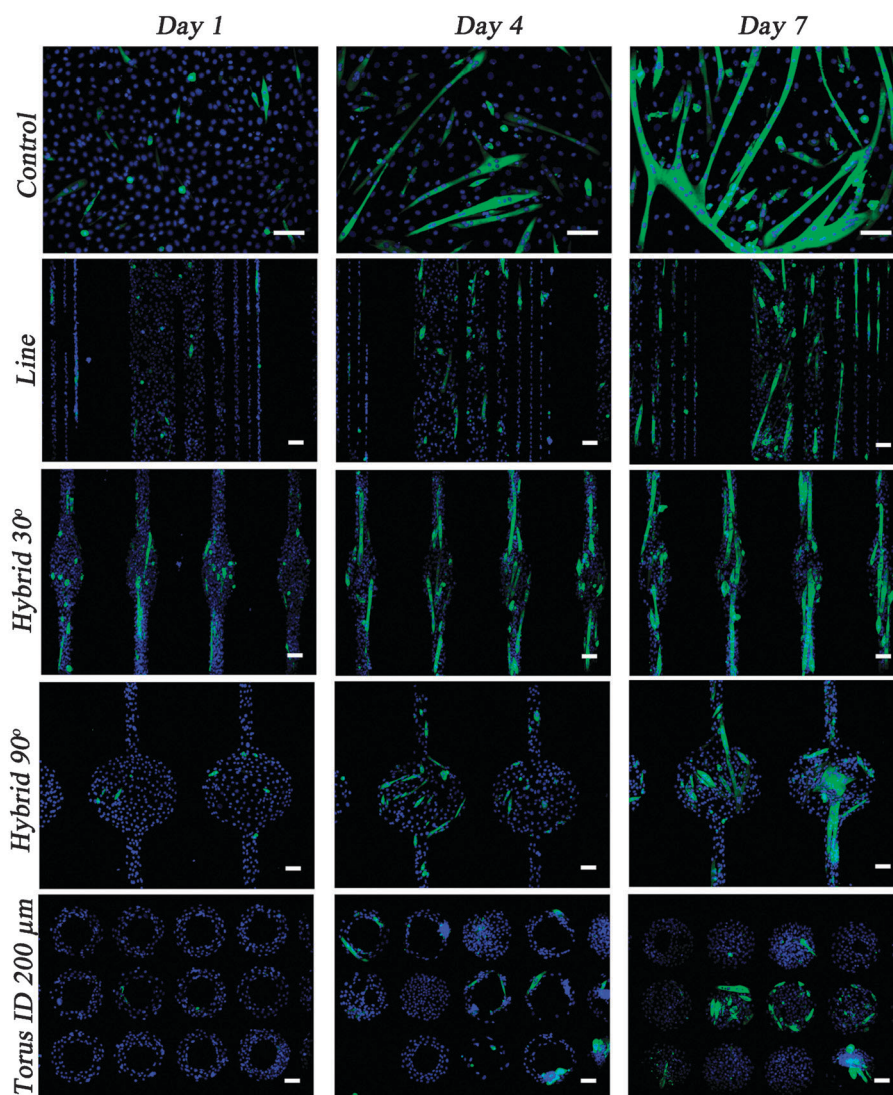
Fig. 2 Fluorescent images of the C2C12 cells on the different patterns. Column 1 shows the C2C12 cells after one day, column 2 shows the cells after four days and column 3 shows the cells after seven days in the differentiation media. Row 1 shows the C2C12 cells present on the unpatterned (control) surface, row 2 shows them on the linear cell islands, rows 3 and 4 show the cells on hybrid patterns with different arc degrees (30° and 90°) and row 5 shows the cells on toroid cell islands. Cells were stained for anti-MHC (green) and nucleus (blue) and these were used for the calculation of the fusion index and the maturation index (% myotubes $\geq$ 5 nuclei). (Scale bar = 100 μm.)

index for the linear geometry with different widths. There was no statistically significant difference in the size of the myotubes on line patterns of different widths. Also, the toroid patterns showed similar results where no significant difference could be seen in the maturation index for tori of different inner diameters. However, each of them showed smaller maturation for the myotubes when compared to the control. Again, the hybrid 30° pattern emerges as the optimum geometry for myotube maturation showing higher maturation than either the linear or the circular geometry (Fig. 4D).

C2C12 myotube alignment on the micropatterned islands

Controlling the alignment of cells is critical for any tissue engineered graft. *In vivo*, many cells/tissues like neural cells,[45] cardiac muscle,[46] skeletal muscle,[47] corneal tissue,[48] vascular tissue[49,50] have a very high degree of alignment associated with them which in turn enhances their functionality. In particular,

for skeletal and cardiac muscles, alignment of cells is extremely important in order to maximize the contractile power of the tissue. We therefore investigated the alignment of myotubes on the micropatterned cell islands using two-dimensional FFT. For a detailed and excellent discussion on the technique the reader is recommended to look at Ayres *et al.*[51,52]

Fig. 5 shows the alignment of MHC-positive myotubes on the different micropatterns. The second column in the figure is the two-dimensional FFT of the image (or the red selection) which shows the distribution of pixels of different frequencies around the origin. Myotubes on the control (unpatterned) substrate show no distinguishable peak in the two-dimensional FFT alignment plot, indicating that there is no alignment of myotubes on this substrate. This was further confirmed by looking at the angle of deviation of myotubes from the principal axis and only less than 20% myotubes showed 15° or less deviation. It has been shown previously that cells
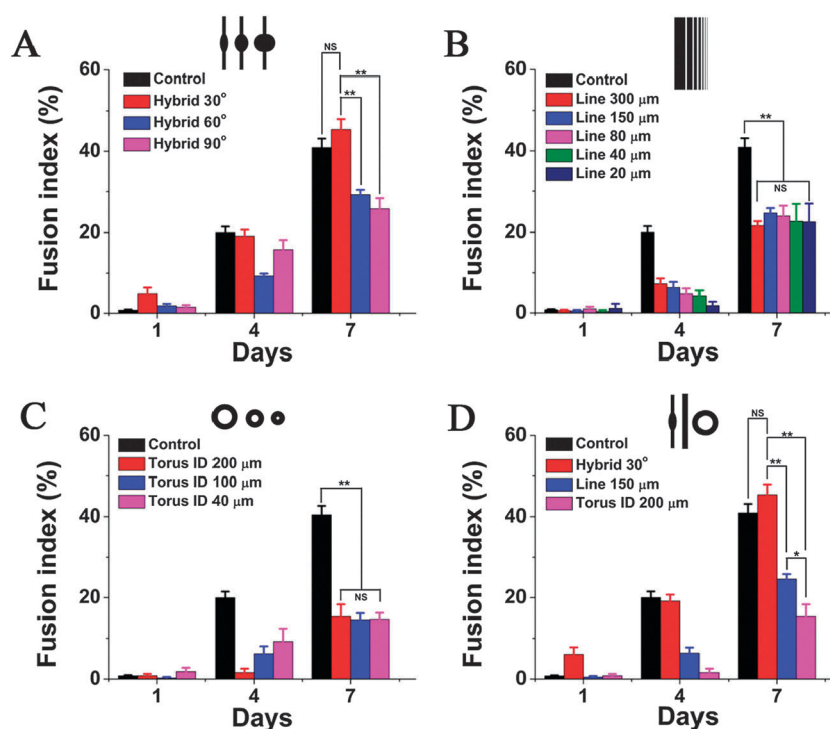
Fig. 3 Quantification of the fusion index for the C2C12 cells on the different micropatterned cell islands. The fusion index was calculated as the ratio of the nuclei number in myocytes with two or more nuclei *versus* the total number of nuclei. (A) Hybrid patterns with different arc degrees (30°, 60°, and 90°). (B) Linear cell islands (line patterns) with different widths (300 μm, 150 μm, 80 μm, 40 μm, and 20 μm). (C) Toroid cell islands (torus patterns) with different inner diameters (40 μm, 100 μm, and 200 μm). (D) The highest from each of the different cell islands are plotted together to show the geometry that maximized the fusion index of C2C12 cells-hybrid 30°. Significance: **$p < 0.01$, *$p < 0.05$, and NS = not significant. Data are represented as mean ± S.E.M. ($n = 10$ patterns).

presenting less than 15° of deviation are considered aligned along the given axis.[53] As expected, myotubes on the linear patterns showed a very high degree of cell alignment. Myotubes on the line (width 80 μm) showed a very sharp narrow peak which is indicative of high degree of cell alignment. More than 90% of the myotubes showed less than 15° of deviation from the principal (long) axis of the linear geometry. However, as the width of the linear geometry was increased from 80 μm to 300 μm, a sharp decrease in the alignment of myotubes was seen. Less than 40% of the myotubes now showed 15° or less of cellular deviation. Also, the two-dimensional FFT alignment plot is now much broader which indicates more than one axis of alignment. By quantifying the alignment of myotubes on the hybrid patterns, we see that hybrid 30° patterns (width of the linear portion is about 100 μm) which showed the highest fusion and the maturation index for the myotubes also showed a very high degree of myotube alignment. Almost 90% of the myotubes showed 15° or less of deviation while 100% of the myotubes were within 30° of deviation from the principal axis of the geometry. The two-dimensional FFT alignment plot also showed a narrow high peak indicating a high degree of alignment for the myotubes. However, the alignment of myotubes for the hybrid 90° patterns (width of the linear portion is about 100 μm) was not very high. Less than 30% of the myotubes showed ≤15° of deviation from the principal axis of the geometry and the two-dimensional FFT alignment plot did not show peaks.

Taken together, these results suggest that as the width of the linear portion in the geometry is increased, the degree of

alignment goes down. Also, by adding a curvature to the linear geometry, the degree of alignment decreases. However, for small curvatures, the deviation is small as seen for the hybrid 30° pattern. As the arc degree of the curvature increases the alignment decreases substantially as seen for the hybrid 90° pattern.

Electrical actuation of mature myotubes

Muscles being an electrogenic tissue, their development is closely linked to their electrical activity. Therefore, we were interested in looking at the contraction of these cells using an electrical pulse stimulator. First, we investigated the effect of frequency on the contraction of myotubes. The myotubes contracted at the rate at which a frequency pulse from the waveform generator was applied to them as seen in Fig. 6A. The data suggest that it is possible to synchronize the frequency of contractions of myotubes to the electrical pulse frequency.

The displacement of myotubes under the application of an electric field for cells on different patterns was quantified. Fig. 6B shows the displacement profile of myotubes on the different patterns on day 7. Twitch responses of myotubes were observed at lower frequencies (1–10 Hz) while tetanic contractions were observed at higher frequencies (≥ 30 Hz). It can be seen from this that the cells showed very uniform displacement under the application of the electric field. The displacement amplitude slightly increased from day 4 to day 7 for all the different patterns as can be seen in Fig. 6C.
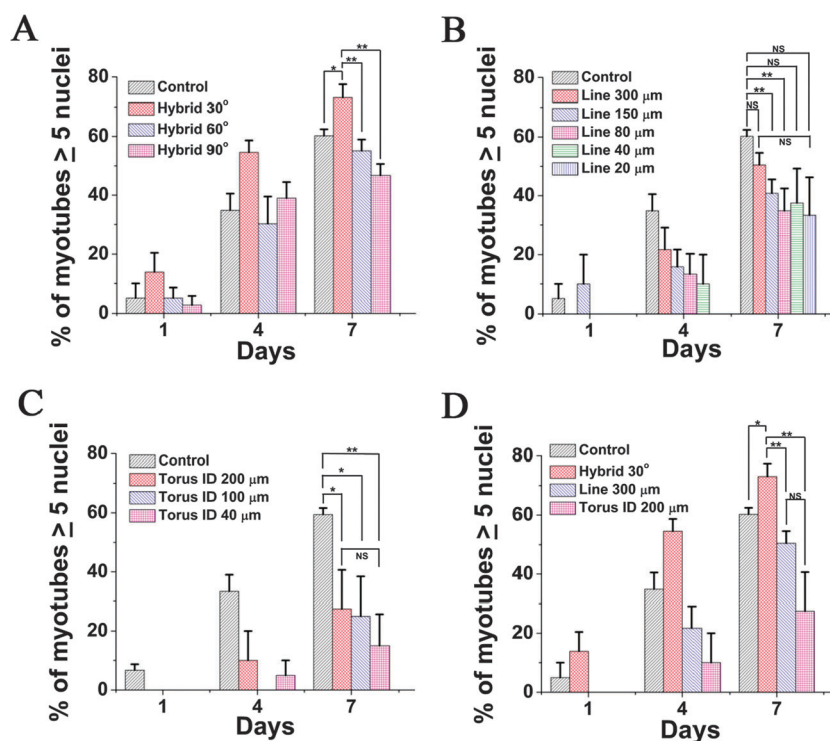
Fig. 4 Quantification of the maturation index (% myotubes with ≥ 5 nuclei) for the C2C12 cells on the different micropatterned cell islands. (A) Hybrid patterns with different arc degrees (30°, 60°, and 90°). (B) Linear cell islands (line patterns) with different widths (300 μm, 150 μm, 80 μm, 40 μm, and 20 μm). (C) Toroid cell islands (torus patterns) with different inner diameters (40 μm, 100 μm, and 200 μm). (D) The highest from each of the different cell islands are plotted together to show the geometry that maximized the fusion index of C2C12 cells-hybrid 30°. In each of the cases, cells present on the unpatterned (control) substrate were also plotted. Significance: **$p < 0.01$, *$p < 0.05$, and NS = not significant. Data are represented as mean ± S.E.M. ($n = 10$ patterns).

The highest displacement was seen for the hybrid 30° pattern with the average being 1.24 ± 0.16 μm. The line pattern (width 300 μm) showed the second highest displacement which was 0.71 ± 0.09 μm followed by the torus (ID 200 μm) pattern which registered an average of 0.60 ± 0.09 μm displacement. Patterns with higher fusion/maturation index showed higher displacements.

Effect of cell density on the fusion and maturation indices

The same numbers of cells were seeded on each of the substrates (initial seeding density was the same on all patterns), but the outcome shows different cell densities for each pattern. This could be attributed to the different areas and different numbers of patterns on each chip. Messina *et al.* showed that myogenesis *in vitro* follows a phenomenon known as the "community effect" where the initial cell density of the myoblast plating is important.[54] When C2C12 myoblasts were seeded at low cell densities (LD, 500 cells per cm^2) compared to high cell densities (HD, 20 000 cells per cm^2) they showed very different fusion indices where LD cultures showed less than 10% MHC positive nuclei while HD cultures showed more than 80% MHC positive nuclei after 72 hours in the DM.

Fig. 7A shows the average cell density on the different patterns plotted together with the fusion index for day 7. The hybrid 30° pattern showed the highest average cell density and the highest fusion index. The inset for Fig. 7A shows cell density plotted against the fusion index of cells. Pearson's

correlation coefficient is 0.495 which suggests that there is a very low level of associativity between the fusion index and cell density. Even though the highest cell density showed the highest cell fusion, density cannot be the dominant factor because of the differences in the fusion indices seen on the different patterns. For example, there is a statistically significant difference between the fusion index of the hybrid 30° and the hybrid 60° pattern at $p < 0.01$. However, for the two same geometries, there is no significant difference in the density. In contrast, the linear geometries (20 μm *versus* 150 μm) show no significant difference in the fusion indices while there is a statistically significant difference in the densities between these two different structures. The same argument also holds true for Fig. 7B where the cellular density and the maturation index are plotted against the type of pattern while the inset shows them plotted against each other. Pearson's correlation coefficient is 0.551 which means that there is low associativity between the two parameters—the maturation index and cellular density. Fig. S6 (ESI†) shows the density of myotubes on the various patterns as a function of time. Under our given experimental conditions we can conclude that the effects of the maturation index and the fusion index on the different patterns are not likely to be attributed to the differences in densities on those patterns. Rather, the data suggest that other inherent mechanisms and cellular pathways exert a dominant influence on this fusion and maturation process for different micropatterned geometries.

After performing a thorough analysis of the different parameters important for the differentiation of C2C12
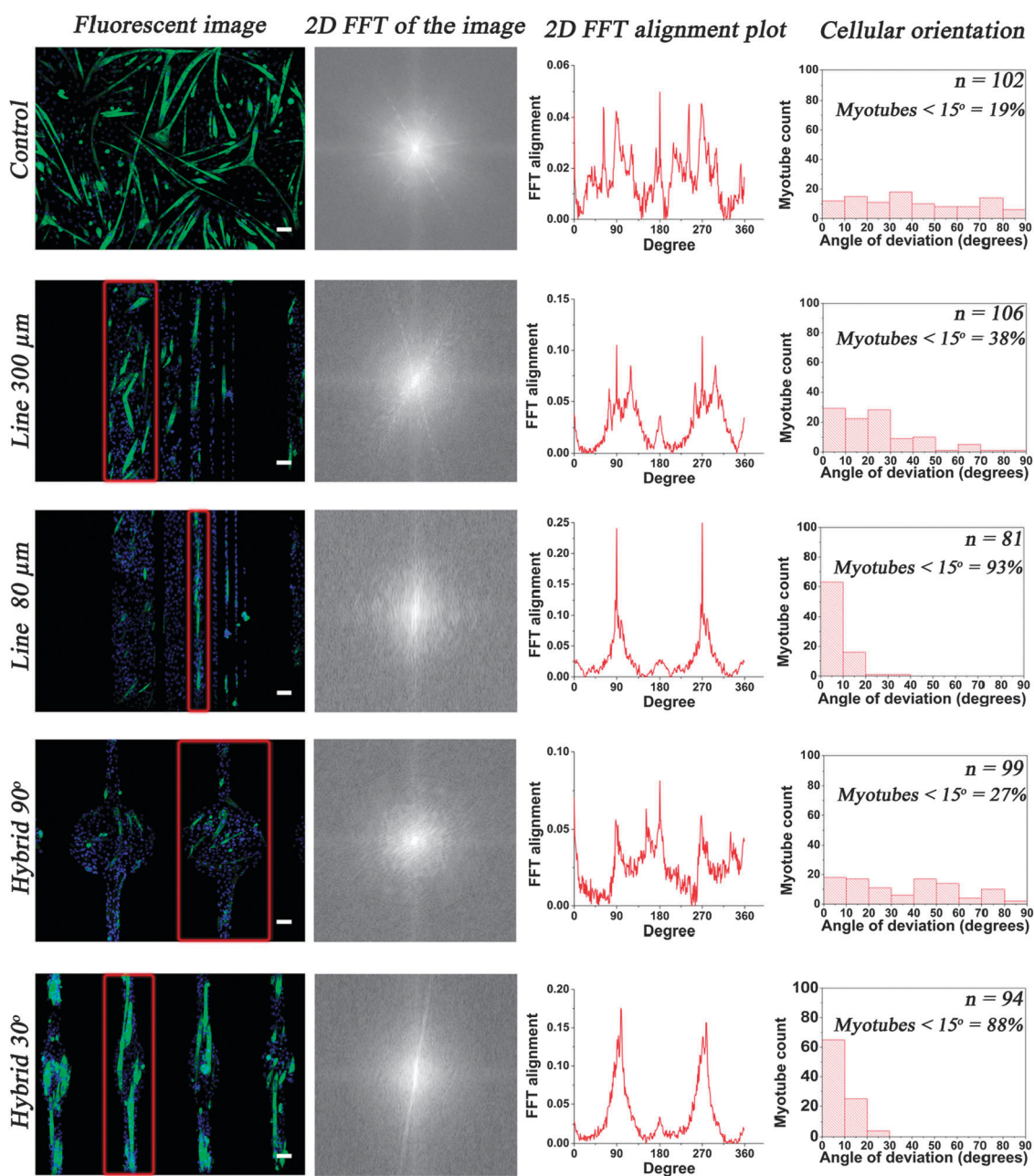
Fig. 5 Quantification of alignment of C2C12 cells on the micropatterned cell islands. The alignment of cells was confirmed using a two-dimensional fast Fourier transform (FFT) of the image. Column 1 shows the fluorescent image of the micropatterned cell island. Column 2 shows the two-dimensional FFT of the image in the first column or the selection (red rectangle) in the image. Column 3 shows the two-dimensional alignment plot which was obtained using ImageJ. Column 4 shows the orientation of cells on the different micropatterned cell islands. ImageJ was used to quantify the angle of deviation of myotubes from the principal axis of the cell islands. n represents the number of myotubes that were used for quantification of cellular orientation of the myotubes. The quantification involved using at least 10 different patterns of each type of geometry for analysis (scale bar = 100 μm).

myoblasts which included fusion index, maturation index, alignment of myotubes and electrical actuation (displacement of myotubes), the hybrid 30° pattern emerges as the optimum geometry in this study.

Discussion

Micropatterning techniques have enabled researchers to print organic molecules on substrates thereby regulating the location and shape of cells on them. Although in two-dimension, μCP allows researchers to study the effect of the micro-environment on the fate of the cell and provides insight into the physiologically complex three-dimensional micro-environment experienced by the cells *in vivo*. In this study, we used μCP to study the differentiation of the murine-derived muscle cell line C2C12 skeletal myoblasts. Geometrical cues conferred by the protein micropatterns possibly lead to different tractional stresses and cytoskeletal reorganization
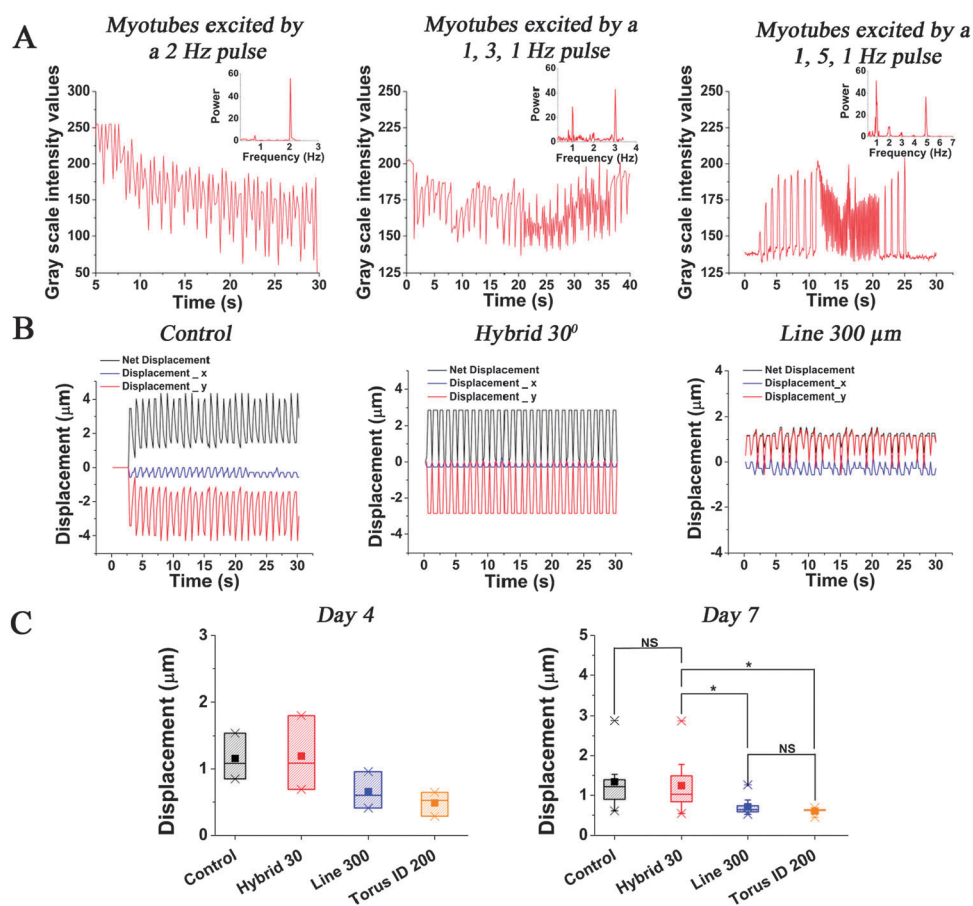
Fig. 6 Quantification of the C2C12 myotubes using the electrical pulse stimulation (EPS) on the different micropatterns. (A) Myotubes were stimulated at different frequencies using the EPS and their response was recorded *via* a kymograph. The grayscale values obtained from the kymograph are plotted as a function of time. The inset shows the spectral density of the signal (power spectrum) obtained from the kymograph by FFT. (B) Time course of maximum contractile displacement of the myotubes on the control, hybrid 30° and line patterns obtained *via* continuous EPS of the myotubes. (C) Box plots showing the average displacements of the patterns on day 4 ($n = 3$) and day 7 ($n = 5$ for the torus, $n = 7$ for the line (300 μm) and $n = 13$ for control and hybrid 30° patterns). The mean is represented as the solid square in the box plot and the top and bottom (×) show the 99 percentile and 1 percentile respectively. Significance: *$p < 0.05$, and NS = not significant. Data are represented as mean ± S.E.M.
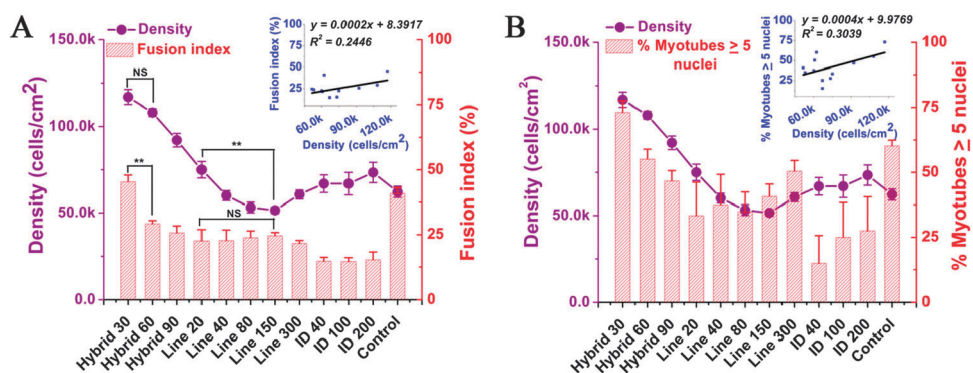
Fig. 7 Influence of density on the differentiation of C2C12 myotubes on the different micropatterns. (A) The fusion index and density of C2C12 myotubes on the various micropatterned cell islands on day 7. The inset shows a scatter plot of the fusion index and the density of C2C12 myotubes. Pearson's correlation coefficient (r) is 0.495 indicating a low association between the fusion index and the density of C2C12 myotubes for day 7. (B) The maturation index (% myotubes $\geq$ 5 nuclei) and density of C2C12 myotubes on the various micropatterned cell islands on day 7. The inset shows a scatter plot of the maturation index and the density of C2C12 myotubes. Pearson's correlation coefficient (r) is 0.551, indicating a low association between the maturation index and the density of C2C12 myotubes for day 7. Significance: **$p < 0.01$, *$p < 0.05$, and NS = not significant. Data are represented as mean ± S.E.M. ($n = 10$ patterns).

of C2C12 cells which caused different degrees of differentiation on the various geometries.

It has been previously shown that the mechanical stress patterns in the micropatterned structures corresponded to cellular growth and proliferation, meaning, higher growth and proliferation of the cell sheet was seen where mechanical stress patterns were high.[9,38] The ratio of the stress between the convex outer edge and the concave inner edge for tori of different IDs (Fig. 1C and Fig. S1B, ESI†) was constant at around 0.5. Since the circumferential area was the least in the smaller ID torus (ID 40 μm), we see that even in as early as 24 hours, the cells proliferated to form a complete circle rather than remaining as a torus. During this time, the cells confined only to form a torus for a larger ID torus (ID 200 μm) because of the larger area. However, with time (by day 7 in DM) even on the larger torus (ID 200 μm) some of the structures were filled up to form a circle rather than remaining a torus. As the torus of ID 100 μm is intermediate between the ID 40 μm and ID 200 μm tori, the cellular conformity results for the ID 100 μm at 24 hours are also intermediate with some islands showing central closure reminiscent of the ID 40 μm, while other islands remain open like the ID 200 μm.

It is shown in Fig. 3B and C and 4B and C that the fusion and maturation indices are not statistically different for lines of different widths and tori of different IDs. However, within the same categories of geometric shapes, why we do not see different rates of fusion and maturation? As pointed out by Nelson et al., cellular signals like proliferation and differentiation emanate from the bulk tissue rather than the edges or length.[9] For example, they show that in their study there was a smaller proliferation along the long edge of the rectangle as compared to the square of the same edge length. Therefore, even though the stress values are different on the linear geometries (different width patterns) and circular geometries (tori of different IDs), the overall distribution in stress gradients is very similar on these structures. This leads to very similar fusion and maturation indices on linear (different width patterns) and circular (tori of different IDs) geometries. Hence, the data suggest that it is not a particular stress value but the stress gradient (distribution of stress) in a structure that dictates the differentiation process.

Studies have shown the alignment of myotubes by modulating the surface topography for instance using grooves/ridges,[55] by grinding the substrate with abrasives,[56] by using UV-lithography to micropattern glass[30] and others.[57,58] In our study, alignment of cells was achieved on different geometries by using μCP in contrast to creating wells/channels for guiding the cells in them. Alignment of cells in wells/channels is because of the topography of the substrate while alignment of cells on the micro contact patterned substrate is because of the chemical patterns.

Chemical patterns differ from topographic patterns in the sense that topographic features do not limit the area for cellular extension and hence the area of cell contact remains unrestricted.[58] Depending on the size of the channels, cell extension can follow "gap guidance" or "contact guidance". On the other hand, in the chemical patterns the area of cell contact is limited by the cell patterns and in general, the cells cannot cross the boundary between the adhesive and non-adhesive cell islands. Alignment of cells is extremely important for skeletal tissue engineering applications as the in vivo skeletal muscle is formed by a highly aligned structure consisting of parallel arrays of multinucleated myotubes. This requires the remodeling of the actin cytoskeleton such that the actin filaments are now aligned parallel to the long (principal) axis of the micropattern which in turn can also affect the differentiation of myotubes.

Alignment of myotubes also imparts anisotropy to the skeletal muscle tissue so that the contractile power of the muscle is maximized. As expected, linear geometries with smaller line widths showed a high degree of alignment. However, the hybrid 30° geometry, which combined both linear and circular features together in a single geometry, also showed a very high degree of alignment. This combined with the fact that hybrid 30° also showed the highest fusion and maturation indices makes it emerge as a promising geometry for studies involving other cell types like hMSCs, embryonic stem cells (ESCs) and induced pluripotent stem cells (iPS) where both differentiation and alignment of the cells/tissue are required.

Myotubes or muscles are linear actuators where the biochemical energy from the cell culture medium is converted into mechanical motion by the actomyosin motors in the cell. As a result, these cells have become strong candidates for many BioMEMS. There have been several examples of using cardiac and skeletal muscle cells for "lab on a chip" applications.[59–63] For all contraction studies, the direction of the electrical field was parallel to the direction of the long axis (longitudinal direction) of the patterns as it has been shown previously that smaller electrical energy is required when the electric field is parallel to the longitudinal axis of the myotubes compared to being perpendicular to it.[44] As shown in Fig. 6A, it is possible to synchronize the frequency of contractions of myotubes to the electrical pulse frequency which can have several applications in the field of BioMEMS like using a tissue engineered system of myotubes as an artificial pump for "lab on a chip" applications.

A very simple explanation to why we see a greater differentiation activity on the hybrid 30° pattern is that it combines the best of the linear (high degree of myotube alignment) and circular (high density) geometries. But in order to get a more mechanistic understanding of this process it is necessary to look at the molecular pathways and molecules that might be involved. However, it was very difficult in this study to point out a single molecule that might be responsible for upregulation of myogenesis on a particular geometry as there are 32 known molecules that are involved in the mammalian process of myoblast fusion.[64] These can be broadly classified into three major types namely membrane-associated proteins, intracellular molecules and extracellular/secreted molecules. It is well known that there are four known muscle regulatory factors (MRFs)—MyoD, Myf-5, myogenin and MRF4 that are involved in in vitro myogenesis.[65,66] Since MyoD and Myf-5 are "commitment" or "specification" factors, myogenin is a "differentiation" factor and MRF4 has both aspects, one or more of the 32 molecules involved in skeletal myogenesis target these four MRFs at different stages of myogenesis leading to differences in differentiation on the different geometries.

Conclusion

Protein micropatterning can be used to mimic, at a fundamental level, the *in vivo* architecture of the tissues and to study cellular differentiation *in vitro*. We conclude that geometrical cues influence the differentiation process of C2C12 myoblasts. We investigated the differentiation of C2C12 myoblasts on three main geometries—a linear, a circular and a hybrid pattern—which combined linear and circular features together in one geometrical unit. The hybrid 30° pattern emerged as the most optimum geometry to maximize the differentiation of C2C12 myotubes. These results can have implications in engineering skeletal muscle tissues and designing muscle cell bio-actuators.

References

1 C. S. Chen, J. Tan and J. Tien, *Annu. Rev. Biomed. Eng.*, 2004, **6**, 275–302.
2 A. Kumar and G. M. Whitesides, *Appl. Phys. Lett.*, 1993, **63**, 2002–2004.
3 G. M. Whitesides, E. Ostuni, S. Takayama, X. Jiang and D. E. Ingber, *Annu. Rev. Biomed. Eng.*, 2001, **3**, 335–373.
4 Y. Xia and G. M. Whitesides, *Annu. Rev. Mater. Sci.*, 1998, **28**, 153–184.
5 A. Folch and M. Toner, *Annu. Rev. Biomed. Eng.*, 2000, **2**, 227–256.
6 C. S. Chen, M. Mrksich, S. Huang, G. M. Whitesides and D. E. Ingber, *Science*, 1997, **276**, 1425–1428.
7 R. McBeath, D. M. Pirone, C. M. Nelson, K. Bhadriraju and C. S. Chen, *Dev. Cell*, 2004, **6**, 483–495.
8 S. A. Ruiz and C. S. Chen, *Stem Cells*, 2008, **26**, 2921–2927.
9 C. M. Nelson, R. P. Jean, J. L. Tan, W. F. Liu, N. J. Sniadecki, A. A. Spector and C. S. Chen, *Proc. Natl. Acad. Sci. U. S. A.*, 2005, **102**, 11594–11599.
10 N. Q. Balaban, U. S. Schwarz, D. Riveline, P. Goichberg, G. Tzur, I. Sabanay, D. Mahalu, S. Safran, A. Bershadsky, L. Addadi and B. Geiger, *Nat. Cell Biol.*, 2001, **3**, 466–472.
11 P. Bajaj, X. Tang, T. A. Saif and R. Bashir, *J. Biomed. Mater. Res., Part A*, 2010, **95**, 1261–1269.
12 D. E. Discher, P. Janmey and Y. L. Wang, *Science*, 2005, **310**, 1139–1143.
13 A. J. Engler, M. A. Griffin, S. Sen, C. G. Bönnemann, H. L. Sweeney and D. E. Discher, *J. Cell Biol.*, 2004, **166**, 877–887.
14 K. Kim, D. Dean, J. Wallace, R. Breithaupt, A. G. Mikos and J. P. Fisher, *Biomaterials*, 2011, **32**, 3750–3763.
15 J. Solon, I. Levental, K. Sengupta, P. C. Georges and P. A. Janmey, *Biophys. J.*, 2007, **93**, 4453–4461.
16 T. Yeung, P. C. Georges, L. A. Flanagan, B. Marg, M. Ortiz, M. Funaki, N. Zahir, W. Y. Ming, V. Weaver and P. A. Janmey, *Cell Motil. Cytoskeleton*, 2005, **60**, 24–34.
17 K. A. Kilian, B. Bugarija, B. T. Lahn and M. Mrksich, *Proc. Natl. Acad. Sci. U. S. A.*, 2010, **107**, 4872–4877.
18 N. F. Huang, S. Patel, R. G. Thakar, J. Wu, B. S. Hsiao, B. Chu, R. J. Lee and S. Li, *Nano Lett.*, 2006, **6**, 537–542.
19 L. H. Lee, R. Peerani, M. Ungrin, C. Joshi, E. Kumacheva and P. Zandstra, *Stem Cell Res.*, 2009, **2**, 155–162.
20 N. Gjorevski and C. M. Nelson, *Integr. Biol.*, 2010, **2**, 424–434.
21 V. Vogel and M. Sheetz, *Nat. Rev. Mol. Cell Biol.*, 2006, **7**, 265–275.
22 I. Delgado, X. Huang, S. Jones, L. Zhang, R. Hatcher, B. Gao and P. Zhang, *Genomics*, 2003, **82**, 109–121.
23 M. Kitzmann, G. Carnac, M. Vandromme, M. Primig, N. J. C. Lamb and A. Fernandez, *J. Cell Biol.*, 1998, **142**, 1447–1459.
24 A. Blais, M. Tsikitis, D. Acosta-Alvear, R. Sharan, Y. Kluger and B. D. Dynlacht, *Genes Dev.*, 2005, **19**, 553–569.
25 B. Li, M. Lin, Y. Tang, B. Wang and J. H. C. Wang, *J. Biomech.*, 2008, **41**, 3349–3353.
26 C. Favreau, E. Delbarre, J.-C. Courvalin and B. Buendia, *Exp. Cell Res.*, 2008, **314**, 1392–1405.
27 A. Fanzani, E. Stoppani, L. Gualandi, R. Giuliani, F. Galbiati, S. Rossi, A. Fra, A. Preti and S. Marchesini, *FEBS Lett.*, 2007, **581**, 5099–5104.
28 K. Shimizu, H. Fujita and E. Nagamori, *J. Biosci. Bioeng.*, 2010, **109**, 174–178.
29 K. Nagamine, T. Kawashima, T. Ishibashi, H. Kaji, M. Kanzaki and M. Nishizawa, *Biotechnol. Bioeng.*, 2010, **105**, 1161–1167.
30 D. L. Yamamoto, R. I. Csikasz, Y. Li, G. Sharma, K. Hjort, R. Karlsson and T. Bengtsson, *J. Histochem. Cytochem.*, 2008, **56**, 881–892.
31 P. Molnar, W. Wang, A. Natarajan, J. W. Rumsey and J. J. Hickman, *Biotechnol. Prog.*, 2007, **23**, 265–268.
32 K. Nagamine, T. Kawashima, S. Sekine, Y. Ido, M. Kanzaki and M. Nishizawa, *Lab Chip*, 2011, **11**, 513–517.
33 E. Cimetta, S. Pizzato, S. Bollini, E. Serena, P. De Coppi and N. Elvassore, *Biomed. Microdevices*, 2009, **11**, 389–400.
34 H. Aubin, J. W. Nichol, C. B. Hutson, H. Bae, A. L. Sieminski, D. M. Cropek, P. Akhyari and A. Khademhosseini, *Biomaterials*, 2010, **31**, 6941–6951.
35 T. Nishiyama, I. Kii and A. Kudo, *J. Biol. Chem.*, 2004, **279**, 47311–47319.
36 L. Castellani, E. Salvati, S. Alemà and G. Falcone, *J. Biol. Chem.*, 2006, **281**, 15249–15257.
37 M. Maekawa, T. Ishizaki, S. Boku, N. Watanabe, A. Fujita, A. Iwamatsu, T. Obinata, K. Ohashi, K. Mizuno and S. Narumiya, *Science*, 1999, **285**, 895–898.
38 B. Li, F. Li, K. M. Puskar and J. H. C. Wang, *J. Biomech.*, 2009, **42**, 1622–1627.
39 M. D. Abramoff, P. Magelhaes and S. J. Ram, *Biophotonics Int.*, 2004, **11**, 36–42.
40 Y. Sun, Y. Ge, J. Drnevich, Y. Zhao, M. Band and J. Chen, *J. CellBiol.*, 2010, **189**, 1157–1169.
41 R. B. Mario Marotta and A. M. Gómez-Foix1, *BioTechniques*, 2004, **36**, 68–73.
42 A. Kamgoué, J. Ohayon, Y. Usson, L. Riou and P. Tracqui, *Cytometry, Part A*, 2009, **75**, 298–308.
43 S. T. Cooper, A. L. Maxwell, E. Kizana, M. Ghoddusi, E. C. Hardeman, I. E. Alexander, D. G. Allen and K. N. North, *Cell Motil. Cytoskeleton*, 2004, **58**, 200–211.
44 K. Yamasaki, H. Hayashi, K. Nishiyama, H. Kobayashi, S. Uto, H. Kondo, S. Hashimoto and T. Fujisato, *J. Artif. Organs*, 2009, **12**, 131–137.
45 J. B. Phillips, S. C. J. Bunting, S. M. Hall and R. A. Brown, *Tissue Eng.*, 2005, **11**, 1611–1617.
46 C. Chung, H. Bien and E. Entcheva, *J. Cardiovasc. Electrophysiol.*, 2007, **18**, 1323–1329.
47 Y. Zhao, H. Zeng, J. Nam and S. Agarwal, *Biotechnol. Bioeng.*, 2009, **102**, 624–631.
48 R. A. B. Crabb, E. P. Chau, M. C. Evans, V. H. Barocas and A. Hubel, *Tissue Eng.*, 2006, **12**, 1565–1575.
49 Y. Zhu, Y. Cao, J. Pan and Y. Liu, *J. Biomed. Mater. Res., Part B*, 2010, **92**, 508–516.
50 P. Bajaj, D. Khang and T. J. Webster, *Int. J. Nanomed.*, 2006, **1**, 361–365.

51 C. Ayres, G. L. Bowlin, S. C. Henderson, L. Taylor, J. Shultz, J. Alexander, T. A. Telemeco and D. G. Simpson, *Biomaterials*, 2006, **27**, 5524–5534.

52 C. E. Ayres, B. S. Jha, H. Meredith, J. R. Bowman, G. L. Bowlin, S. C. Henderson and D. G. Simpson, *J. Biomater. Sci., Polym. Ed.*, 2008, **19**, 603–621.

53 A. S. Crouch, D. Miller, K. J. Luebke and W. Hu, *Biomaterials*, 2009, **30**, 1560–1567.

54 G. Messina, C. Blasi, S. A. La Rocca, M. Pompili, A. Calconi and M. Grossi, *Methods Mol. Biol.*, 2005, **16**, 1469–1480.

55 P. Y. Wang, H.-T. Yu and W.-B. Tsai, *Biotechnol. Bioeng.*, 2010, **106**, 285–294.

56 K. Shimizu, H. Fujita and E. Nagamori, *Biotechnol. Bioeng.*, 2009, **103**, 631–638.

57 T. M. Patz, A. Doraiswamy, R. J. Narayan, R. Modi and D. B. Chrisey, *Mater. Sci. Eng., B*, 2005, **123**, 242–247.

58 J. L. Charest, A. J. García and W. P. King, *Biomaterials*, 2007, **28**, 2202–2210.

59 A. W. Feinberg, A. Feigel, S. S. Shevkoplyas, S. Sheehy, G. M. Whitesides and K. K. Parker, *Science*, 2007, **317**, 1366–1370.

60 Y. Tanaka, K. Morishima, T. Shimizu, A. Kikuchi, M. Yamato, T. Okano and T. Kitamori, *Lab Chip*, 2006, **6**, 362–368.

61 Y. Tanaka, K. Morishima, T. Shimizu, A. Kikuchi, M. Yamato, T. Okano and T. Kitamori, *Lab Chip*, 2006, **6**, 230–235.

62 Y. Akiyama, Y. Furukawa and K. Morishima, Engineering in Medicine and Biology Society, 2006. EMBS '06. 28th Annual International Conference of the IEEE, 2006.

63 H. Herr and R. Dennis, *J. NeuroEng. Rehabil.*, 2004, **1**, 6.

64 K. M. Jansen and G. K. Pavlath, *Methods Mol. Biol.*, 2008, **475**, 115–133.

65 N. Yoshida, S. Yoshida, K. Koishi, K. Masuda and Y. Nabeshima, *J. Cell Sci.*, 1998, **111**, 769–779.

66 M. Kitzmann and A. Fernandez, *Cell. Mol. Life Sci.*, 2001, **58**, 571–579.